

A Quantized Interband Topological Index in Two-Dimensional Systems

Tharindu Fernando*

Department of Physics, University of Washington, Seattle, WA 98195 USA

Ting Cao

Department of Materials Science and Engineering,
University of Washington, Seattle, WA 98195 USA

(Dated: August 1, 2023)

We introduce a novel gauge-invariant, quantized interband index in two-dimensional (2D) multi-band systems. It provides a bulk topological classification of a submanifold of parameter space (e.g., an electron valley in a Brillouin zone), and therefore overcomes difficulties in characterizing topology of submanifolds. We confirm its topological nature by numerically demonstrating a one-to-one correspondence to the valley Chern number in $k \cdot p$ models (e.g., gapped Dirac fermion model), and the first Chern number in lattice models (e.g., Haldane model). Furthermore, we derive a band-resolved topological charge and demonstrate that it can be used to investigate the nature of edge states due to band inversion in valley systems like multilayer graphene.

Topological and geometric effects are being heavily investigated in contemporary condensed matter physics. For an adiabatic evolution along a closed loop in a 2D parameter space, the geometric part of the final electronic eigenstate's phase is $U(1)$ gauge-invariant (modulo 2π). This Berry phase contribution depends solely on the geometry of the parameter space [1]. The corresponding Berry curvature is a geometrically local quantity, which when summed over the entire 2D-space manifold, may yield topological quantities such as the first Chern number [2–4]. In solid state physics, the Berry phase also plays vital roles in topology-related phenomena, and applications including electric polarization, orbital magnetism, adiabatic charge pumping, various types of Hall effects, and edge state engineering [5, 6].

Despite these advancements, the understanding of the multi-level topology of parameter-space submanifolds is arguably still under development. This Article will focus on k -space submanifolds in the vicinity of band edges at high-symmetry points (or so-called *valleys*) [7]. These valley degrees of freedom play key roles in future electronics and quantum information science, as quasiparticles residing in the valleys may carry information much like charge and spin [7–27]. The associated topology is currently studied using the *valley Chern number*. This is usually calculated using a loop integral of the Berry connection (a method that is arguably restrictive due to requiring a non-singular gauge), or by integrating Berry curvature, in the vicinity of a valley [5]. Generally, both $k \cdot p$ and lattice models have proven useful in the study of topological phenomena of valleys. However, in $k \cdot p$ models, the area of Berry curvature integration required to obtain quantized valley Chern number is infinite (or equivalently, requires an infinitesimally small band gap [5, 7, 22]). On the other hand, in lattice models, there is no general quantized character to describe valley topol-

ogy when the Berry curvature is not peaked at the valley; at least not without low-energy expansions or additional synthetic dimensions [6, 28]. In addition, relating existing bulk indices to edge modes by the bulk-edge correspondence often requires summing the valley Chern number over all filled bands [5], and/or downfolding multiband Hamiltonians into simpler models [29–31]. This may cause a loss of information on the topological origin of edge states. For example, if the edge state arises from inverting a pair of bands among many bands, such band-resolved information would be missing in the valley Chern number description.

In this Article, we introduce a new topological index Θ , and the *interband frequency*; a correction term that keeps Θ quantized. Our approach gives us a *meaningful* topological valley index using a *finite* k -space integration, in *both* $k \cdot p$ and lattice models. We also present a band-resolved topological charge Ξ , that identifies orbitals associated with band inversions *without* downfolding multiband Hamiltonians.

Interband index in 2D.—Consider the time-independent Schrödinger equation for an N -level non-degenerate Hamiltonian $H(\mathbf{k})$ over 2D parameter space k : $H(\mathbf{k})|m(\mathbf{k})\rangle = E_m(\mathbf{k})|m(\mathbf{k})\rangle$, ($m = 1, 2, \dots, N$), where $|m\rangle$ are orthonormal instantaneous eigenstates with eigenvalues $E_m(\mathbf{k})$. For an adiabatic evolution along a closed k -space loop $\partial\mathcal{M}$, we define the interband index $\Theta_{\mathbf{k}}$, following the definition of the *interlevel character* in Ref. [32]:

$$2\pi\Theta_{mn} = \Delta\Phi_{mn} - \oint_{\partial\mathcal{M}} \text{darg} \langle m | \nabla_{\mathbf{k}} n \rangle \cdot \hat{e}_\tau, \quad (1)$$

Above, we used the definitions: $\mathbf{k} = (k_x, k_y)$; d is the total derivative with respect to k_x and k_y ; $\nabla_{\mathbf{k}} = (\partial_{k_x}, \partial_{k_y})$; $\hat{e}_\tau = \dot{\mathbf{k}}/|\dot{\mathbf{k}}|$ is the unit tangential operator at a point on the loop $\partial\mathcal{M}$ (see Fig. 1 (b)); $\dot{\mathbf{k}} = \text{d}\mathbf{k}(\lambda)/\text{d}\lambda$ for some λ that parameterizes the loop $\mathbf{k} = (k_x(\lambda), k_y(\lambda))$; and $\Delta\Phi_{mn} = \Phi_m - \Phi_n$, where $\Phi_m = \int_{\partial\mathcal{M}} \mathcal{A}_m^\mu \text{d}\lambda_\mu - \iint_{\mathcal{M}} F_m \text{d}\lambda_\mu \text{d}\lambda_\nu$. For brevity, we henceforth drop the

* tharindu@uw.edu

differential elements $d\lambda_\mu$. Φ_m is the number of *Berry singularities* in level $|m\rangle$: It is the difference between the line integral of the standard Berry connection $\mathcal{A}_m^\mu = i\langle m|\frac{\partial}{\partial\lambda_\mu}|m\rangle$ along $\partial\mathcal{M}$, and the area integral of the Berry curvature $F_m = \frac{\partial}{\partial\lambda_\nu}\mathcal{A}_m^\nu - \frac{\partial}{\partial\lambda_\nu}\mathcal{A}_m^\mu$ over the region \mathcal{M} specified by the loop. So, Φ_m could be interpreted as the quantized ‘amount’ by which Stokes’ theorem fails. Then, $\Delta\Phi$ is the net number of Berry singularities between the levels considered. Notice that in the case without gauge singularities, Φ_m reduces to 0 as $\int_{\partial\mathcal{M}}\mathcal{A}_m^\mu = \iint_{\mathcal{M}}F_m$.

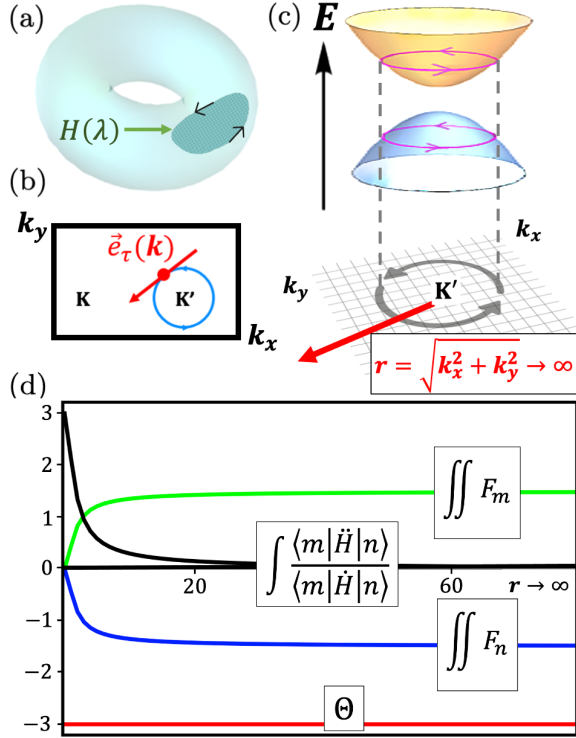


FIG. 1: (a) 2D k -space Brillouin torus for a two-level system. The counterclockwise closed loop is $\partial\mathcal{M}$, and defines the shaded region of the torus as \mathcal{M} , by convention. For a k -space loop parameterized by λ , the adiabatic evolution is given by $H(\lambda) \equiv H(\mathbf{k})$. (b) For k constrained to $\partial\mathcal{M}$, the tangential vector $\vec{e}_\tau(k)$ at a point is denoted in red. K and K' are high-symmetry points. (c) Two energy levels of the dispersion E in the vicinity of the K' valley. The red arrow schematically illustrates how the gray k -space loop’s radius r is increased in (d). (d) Berry curvature area integrals of upper and lower bands, integral of interband frequency, and the interband index in Eq. (2) as we vary the size of k loops using r .

Following the derivation in Supplementary Material

(SM) A, Θ_{mn} may be written as:

$$2\pi\Theta_{mn} = \iint_{\mathcal{M}} F_n - \iint_{\mathcal{M}} F_m - \oint_{\partial\mathcal{M}} \text{Im} \frac{\langle m|\dot{H}|n\rangle}{\langle m|\dot{H}|n\rangle} - \oint_{\partial\mathcal{M}} \sum_{q \neq m,n} \frac{1}{E_{nq}} \left(2 - \frac{E_{nm}}{E_{qm}} \right) \text{Im} \frac{\langle m|\dot{H}|q\rangle\langle q|\dot{H}|n\rangle}{\langle m|\dot{H}|n\rangle}. \quad (2)$$

The overhead dots represent derivation with respect to parameter λ . All terms in Eq. (2) are gauge-independent, and so, potentially observable. The first two terms in the right hand side of Eq. (2) make the difference between the Berry curvature integrals. The third boundary term includes $\langle m|\dot{H}|n\rangle/\langle m|\dot{H}|n\rangle$, which we call the *interband frequency*, since it resembles the ratio of an acceleration-like quantity to a velocity-like quantity. Since $k \rightarrow \infty$ implies the loop-parameter (e.g., time) $\lambda \rightarrow \infty$, we intuit that the frequency ($\propto 1/\lambda$) $\rightarrow 0$. We show later in Fig. 1 (d) that as $k \rightarrow \infty$, this correction term also tends to 0 in our numerical calculations on 2-band models. To our knowledge, the interband frequency is new to the literature. Due to its dependence on the tangential vector \hat{e}_τ , a unique vector field may be defined only *after* a loop is chosen. This makes the individual terms in the interband frequency ratio differ from existing quantities in the literature (such as the interband acceleration in second order nonlinear responses [33, 34]).

The physical significance of the interband index thus becomes clear: It is a quantized topological character for a submanifold of 2D parameter space that depicts the difference between the Berry phases of a pair of bands, corrected by the interband frequency and other terms. Next, we demonstrate the physical meaning and applications of the interband index in $k \cdot p$ and lattice models.

Application to the gapped Dirac fermion model and Haldane model.—We first calculate Θ and compare it with existing topological characterizations of $k \cdot p$ models. While we use the gapped Dirac fermion model for illustration, our results hold for the other systems we tested (SM C). Effective models often follow from low-energy expansions about a high-symmetry point or band extremum P , and can describe important band inversions leading to chiral edge states [6, 9, 10, 12, 17, 18, 22–24]. However, being subspaces of the complete Hilbert space, these models may not have a closed k -space manifold (e.g., 2D Brillouin torus). One significant example is the electron valley degree of freedom. The conventional valley Chern number $\bar{\nu}^P$ is usually given by the k -space integral of the Berry curvature F_m of filled bands in the vicinity of a valley centered at P , integrated to infinity:

$$\bar{\nu}^P = \sum_{i \in \text{filled}} \iint_{k \rightarrow \infty} F_i \equiv \sum_{i \in \text{filled}} \bar{C}_i^P. \quad (3)$$

Above, \bar{C}_i^P is the valley Chern number at P per band $|i\rangle$, and the overhead bar indicates that we used the conventional definition of (3) in contrast to the new definition that we will discuss next. Topological quantities like $\bar{\nu}^P$ are only approximately quantized, unless the range of the

integral in k is infinite. However, using Θ instead of $\bar{\nu}^P$ Eq. (3) gives manifestly *quantized* integers using a *finite* loop about P . This property may be considered advantageous since we do not need an infinite area of integration. Indeed, the relation to topology becomes clear when we show that the interband index is twice the valley Chern number, i.e., $\Theta = 2\bar{\nu}^P$ in 2-band $k \cdot p$ models.

For illustration, consider the 2D gapped Dirac fermion model [35–38], which has a $k \cdot p$ Hamiltonian with integer winding number w :

$$\mathbf{H}(\mathbf{k}) = \begin{pmatrix} \Delta & \alpha|\mathbf{k}|^\gamma e^{iw\phi_k} \\ \alpha|\mathbf{k}|^\gamma e^{-iw\phi_k} & -\Delta \end{pmatrix}, \quad (4)$$

where the energy gap is 2Δ , and $\phi_{\mathbf{k}} = \tan^{-1}(k_y/k_x)$ [39]. The energy dispersions for the upper (m) and lower (n) bands are respectively $\pm\sqrt{\Delta^2 + \alpha^2|\mathbf{k}|^{2\gamma}}$. For a circular loop parameterized as $(k_x, k_y) = (r \cos(\lambda), r \sin(\lambda))$ and centered at the K' point (see Fig. 1 (c)), the first three integrals in Eq. (2) conspire to give quantized Θ . The last term in Eq. (2) does not exist in 2-band models. As the area of integration approaches the limit $k \rightarrow \infty$, the third integral in Eq. (2) contributes less, making Θ the difference in integrals of F_m and F_n . In the $k \rightarrow \infty$ limit, these two integrals are just \bar{C}_m^K and \bar{C}_n^K . We demonstrate this in Fig. 1 (d), where we used $w = 3$, $\Delta = 1$, $\gamma = 1$ and $\alpha = 1$. See SM B for more on the model's Berry curvature.

To verify $\Theta = 2\bar{\nu}^{K'}$, consider the $k \rightarrow \infty$ limit. The Berry curvature sum rule $\sum_i F_i = 0$ gives $F_n = -F_m$ for 2-band models. Since $\bar{\nu}^{K'} = \iint F_n$ in this limit, the claim follows from Eq. (2) since the interband frequency integral tends to 0. Indeed, the figure shows $\iint F_n \rightarrow -1.5 = \bar{\nu}^{K'}$. With $\Theta = -3$, we verify $\Theta = 2\bar{\nu}^{K'}$.

Next, we discuss Θ in lattice models. For demonstration, we use Haldane's 2-band model for the quantum anomalous Hall effect [35]. However, our results hold for all the models tested in SM C. On a honeycomb lattice, its Hamiltonian can be written in a Bloch state basis on two sublattices A, B , using Pauli matrices σ_i . Below, t_1 is the nearest-neighbor hopping, t_2 the amplitude of the complex second-neighbor hopping, ϕ the phase accumulated by the t_2 hopping, and M the on-site energy between the A and B sublattices. \mathbf{a}_i are displacements from a B site to its three nearest-neighbor A sites, and \mathbf{b}_i are displacements for nearest-neighbor sites in the same sublattices [40]:

$$\begin{aligned} \mathbf{H}(\mathbf{k}) = & 2t_2 \cos \phi \left[\sum_i \cos(\mathbf{k} \cdot \mathbf{b}_i) \right] \\ & + t_1 \left[\sum_i [\cos(\mathbf{k} \cdot \mathbf{a}_i)\sigma_1 + \sin(\mathbf{k} \cdot \mathbf{a}_i)\sigma_2] \right] \\ & + \left[M - 2t_2 \sin \phi \left(\sum_i \sin(\mathbf{k} \cdot \mathbf{b}_i) \right) \right] \sigma_3. \end{aligned} \quad (5)$$

This model can give topologically nontrivial first Chern numbers that may yield topologically-protected

edge states [35]. The Chern number $C = \sum_{i \in \text{filled}} \iint_{k \in \text{FBZ}} F_i$ (where FBZ \equiv first Brillouin zone) changes when the band gap closes and reopens at the high-symmetry points (K or K'), as shown in Fig. 2 (a)-(b). The physics at these valleys is therefore significant, because their gap closings can change the topology, and therefore edge state physics. However, unlike with the Dirac fermion model, it is not easy to define an analogous near-quantized topological quantity at valleys in lattice models. This is because the Berry curvature is not necessarily highly localized at P , and the area of the valley available for integration is finite. Therefore, quantities like $\bar{\nu}^P$ cannot often be directly acquired from lattice models; at least not without low-energy expansions.

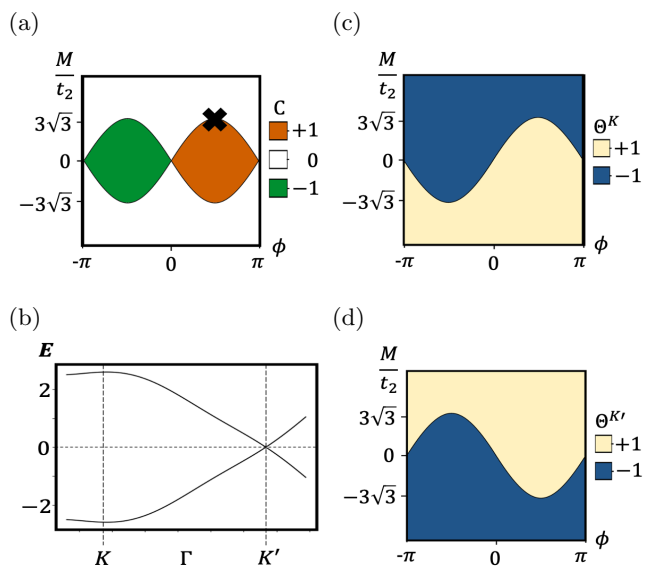


FIG. 2: (a) A phase diagram of the first Chern number C for the Haldane model as a function of (M, ϕ) . The topological phase transitions occur by gap closures at K or K' . (b) Conduction and valence bands of the Haldane model for $M/t_2 = 3\sqrt{3}$, $\phi = \pi/2$, and $t_1 = 4t_2 = 1$. The gap closure at K' corresponds to the phase boundary marked with a cross \times in (a). (c) $\Theta^K(M/t_2, \phi)$ using a fixed k -space loop of radius 0.2 around the K point (d) $\Theta^{K'}(M/t_2, \phi)$. Notice that $\Theta^K(M/t_2, \phi) + \Theta^{K'}(M/t_2, \phi) = 2C(M/t_2, \phi)$, which is exactly twice the expected phase diagram (a).

However, Θ can again provide a quantized valley characterization using a small loop centered at P . Figures 2 (c)-(d) show ‘phase diagrams’ analogous to Fig. 2 (a), but showing Θ for each valley. Clearly, when Θ^K and $\Theta^{K'}$ are summed at each phase space $(M/t_2, \phi)$ point in Fig. 2 (c) and (d), we recover Haldane’s phase diagram Fig. 2 (a): $\Theta^K + \Theta^{K'} = 2C$ [41]. Hence, compared to the state of the art, we now have a tool to analyze each valley in lattice models without using low-energy expansions.

Band-resolved topological charge.—The connections

between the interband index and local topological characteristics motivate us to define a band-resolved topological charge Ξ^P for each P that would add up to the Chern number C . For example, in the Haldane mode, we can define $\Xi^K + \Xi^{K'} \equiv \Theta^K/2 + \Theta^{K'}/2 = C$. This band-resolved topological charge can be generalized to valley and multiband problems. This allows us to not only calculate band-resolved and valley topological indices, but also to identify the number and source of edge states from inverting bulk bands without downfolding.

To make this multiband functionality apparent, we use Θ_{mn} (Eq. (1)) to define the novel generalized band-resolved topological charge Ξ_i^γ per band $|i\rangle$, of context γ (e.g., γ could be P , such as K). For an N -level Hamiltonian, the N possible Ξ_i^γ values may be found by solving the overdetermined simultaneous equations:

$$\{\Theta_{mn}^\gamma = \Xi_n^\gamma - \Xi_m^\gamma, \quad \sum_i \Xi_i^\gamma = 0\}. \quad (6)$$

We choose $N - 1$ of the $N(N - 1)/2$ equations involving Θ_{mn}^γ that make an appropriate linearly independent subset of equations along with $\sum_i \Xi_i^\gamma = 0$, which is a *conservation condition* that resolves linear dependence. This conservation condition is analogous to the Berry curvature sum rule: for a complete basis, the topological charges should sum to 0. Notice that since Θ_{mn}^γ is always an integer, it is reasonable to expect Ξ_i^γ to be rational.

Motivated by how $\bar{\nu}^P$ is a sum over filled bands (Eq. (3)), we define [42]:

$$\nu^\gamma = \sum_{i \in \text{filled}} \Xi_i^\gamma. \quad (7)$$

We numerically find that Ξ_i^γ and ν^γ are sufficient to calculate the number of edge modes, without using conventional topological quantities such as the Chern number and valley Chern number. By the bulk-edge correspondence, the number of edge modes b due to a domain boundary separating two systems α and β is $b = |T^\alpha - T^\beta|$, where T^γ is some topological character for context γ . For example, two adjacent Chern insulators give: $b = |C^\alpha - C^\beta|$ [6]. Or, for a domain boundary between two valleys [43], we have: $b = |\nu^K - \nu^{K'}|$ (Eq. (7)) [26, 27]. And if the boundary is due to two bulk systems with different external potentials U_1 and U_2 at the same P , we get: $b = |\nu^{P,U_1} - \nu^{P,U_2}|$ [26]. Our numerical results shown next support these claims.

We first exemplify the quantities we introduced using the gapped Dirac fermion model (Eq. (4)). For the example in Fig. 1 (d), we use $\Theta = -3$ and solve the simultaneous equations $\{-3 = \Xi_n - \Xi_m, \Xi_n + \Xi_m = 0\}$ (Eq. (6)) to get $\Xi_n = -1.5$ and $\Xi_m = 1.5$, which is consistent with the conventional valley Chern number per band (Eq. (3) $\bar{C}_n^K \approx -1.5$ and $\bar{C}_m^K \approx 1.5$; see Fig. 1 (d)).

For a multiband example, consider the 8-band model for gated bilayer graphene including Rashba spin-orbit coupling ([26]; parameter values in SM F). As the spin-orbit coupling parameter is tuned from $\lambda_R = 0.2t$ to $0.4t$,

	Ξ_A	Ξ_B	Ξ_C	Ξ_D	Ξ_E	Ξ_F	Ξ_G	Ξ_H
$\Xi_i^{0.4}$	$-\frac{1}{2}$	$\frac{1}{2}$	$-\frac{3}{2}$	$\frac{1}{2}$	$-\frac{1}{2}$	$\frac{3}{2}$	$-\frac{1}{2}$	$\frac{1}{2}$
$\Xi_i^{0.2}$	$-\frac{1}{2}$	$\frac{1}{2}$	$-\frac{3}{2}$	$-\frac{1}{2}$	$\frac{1}{2}$	$\frac{3}{2}$	$-\frac{1}{2}$	$\frac{1}{2}$

TABLE I: $\Xi_i^{\lambda_R}$ for the K valley of the 8-band model for gated bilayer graphene. At K' , $\Xi_i^{\lambda_R, K'} = -\Xi_i^{\lambda_R, K}$.

we expect a band inversion at the K valley [26], as in Fig. 3 (a). For these two values of λ_R , we present Ξ_i in Table I.

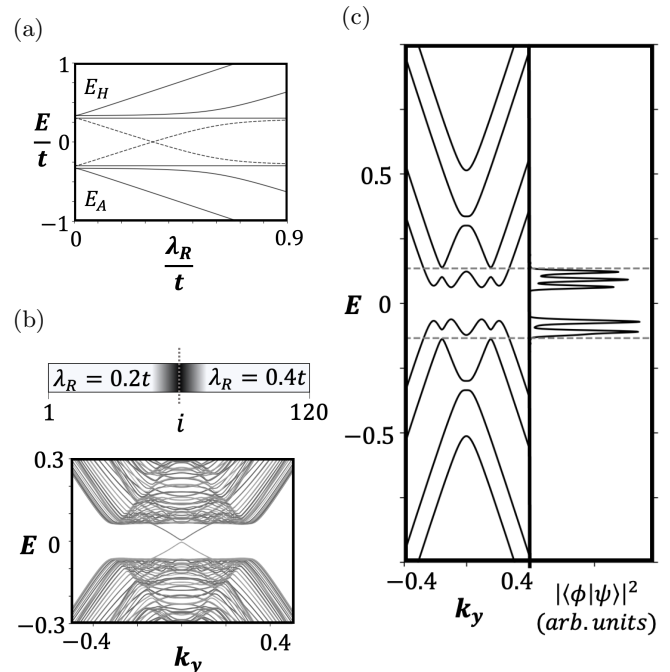


FIG. 3: (a) Band diagram at the K point $(k_x, k_y) = (0, 0)$ for the 8-band bilayer graphene model. At $\lambda_R = 0.2t$, the bands are labeled E_A, E_B, \dots, E_H as we go from -1 to $+1$ along the vertical axis. As λ_R is varied from $0.2t$ to $0.4t$, the bands E_D and E_E invert at $\lambda_R \approx 0.33t$. (b) *Top*: Schematic of real-space nanoribbon with a domain boundary in the x -direction separating regions of two different λ_R . The shaded area represents the calculated wavefunction density. *Bottom*: Nanoribbon bands at $k_x = 0$ along the k_y direction. (c) *Left*: Bulk bands at $k_x = 0$ for $\lambda_R = 0.2t$. *Right*: Gaussian-broadened overlap element between bulk and domain boundary band wavefunctions $|\langle \phi | \psi \rangle|^2$.

We map the $\Xi_i^{\lambda_R}$ in Table I to existing topological quantities: First, we see that for each choice of λ_R , $C = \nu^K + \nu^{K'} = 0$, due to $\Xi_i^{\lambda_R, K'} = -\Xi_i^{\lambda_R, K}$. This is consistent with the time-reversal symmetry of the model. We note that the limit of each \bar{C}_i^P may not tend to the quantized Ξ_i in N -band models with

$N > 2$. To see this, we calculated \bar{C}_i^P at valley K in the $k \rightarrow \infty$ limit using Eq. (3). For $\lambda_R = 0.2t$, $(\bar{C}_A^K, \bar{C}_B^K, \bar{C}_C^K, \bar{C}_D^K, \dots) \approx (-0.01, 0.99, -1.99, -0.99, \dots)$. We see that $\bar{C}_A \approx -0.01 \rightarrow 0$, which is different from $\Xi_A = -1/2$. This mismatch arises from the last two correction terms in Eq. (2), which do not necessarily tend to 0 in models with $N > 2$ bands.

However, a difference between indices may indicate the number of edge states. Consider a valley problem with a domain boundary between K and K' for fixed λ_R at half-filling. From Table I, we have $b = |\nu^K - \nu^{K'}| = |-1 - 1| = 2$ for $\lambda_R = 0.4t$, and $b = |-2 - 2| = 4$ for $\lambda_R = 0.2t$. If we instead take a domain boundary problem at K for the two λ_R values, we get $b = |\nu^{0.4} - \nu^{0.2}| = |-1 - (-2)| = 1$ as the number of edge modes due to the band inversion. These results are consistent with Ref. [26].

We also show that Ξ_i can identify the bulk bands and orbitals causing edge states without explicitly tracking the evolution of spectra (as done in Fig. 3 (a)). Since the only indices that differ between $\lambda_R = 0.4t$ and $\lambda_R = 0.2t$ are Ξ_D and Ξ_E , the orbitals causing edge states are from bands E_D and E_E . To verify this, we further model a tight-binding nanoribbon of 120 sites that is periodic in the y -direction, that has a domain boundary in the x -direction at site $i = 60$, as in Fig. 3 (b) (top). We discretized the continuum model Eq. (F1) to get a tight-binding model that includes both valleys. Our calculations [44] show that edge states accumulate at the domain boundary. We then calculated

the nanoribbon bands in Fig. 3 (b) (bottom), which shows one zero-energy edge state from each valley. Fig. 3 (c) shows that these edge states are composed of orbitals from E_D and E_E , evident from the large overlap between the zero-energy edge state wavefunction $|\phi\rangle$ and the bulk wavefunctions $|\psi\rangle$ of E_D and E_E (calculated in a homogeneous nanoribbon at $\lambda_R = 0.2t$).

Conclusion and outlook.—We introduced two gauge-invariant quantities, the interband index Θ_{mn} and band-resolved topological charge Ξ_i . These quantized indices offer novel characterizations of topologically significant submanifolds in 2D k -space manifolds that are consistent with existing topological characters such as the first and valley Chern numbers. As demonstrated, the differences between Ξ values from different contexts may carry desired physical meaning as the number of edge states. So, the universality and significance of individual Ξ warrant further investigation, as does the interpretation of Θ and Ξ for loops not enclosing a single P (see SM E). The non-Abelian version of the interlevel index provided in Ref. [32] may be extended to treat degeneracies, and deserves further work due to the prevalence of accidental and symmetry-protected degeneracies in condensed matter systems. In conclusion, these first-in-literature quantities, due to their elegant, quantized nature and broad applicability, are prime candidates for deeper study.

We acknowledge helpful discussions with Chao Xu from UC San Diego, and with Yafei Ren and Di Xiao from the University of Washington.

-
- [1] M. V. Berry, Quantal phase factors accompanying adiabatic changes, *Proceedings of the Royal Society of London. A. Mathematical and Physical Sciences* **392**, 45 (1984).
- [2] D. J. Thouless, M. Kohmoto, M. P. Nightingale, and M. den Nijs, Quantized hall conductance in a two-dimensional periodic potential, *Physical Review Letters* **49**, 405 (1982).
- [3] B. Simon, Holonomy, the quantum adiabatic theorem, and berry's phase, *Physical Review Letters* **51**, 2167 (1983).
- [4] M. Nakahara, *Geometry, topology and physics* (CRC press, 2018).
- [5] D. Xiao, M.-C. Chang, and Q. Niu, Berry phase effects on electronic properties, *Reviews of Modern Physics* **82**, 1959 (2010).
- [6] M. Z. Hasan and C. L. Kane, Colloquium: topological insulators, *Reviews of Modern Physics* **82**, 3045 (2010).
- [7] X. Fan, T. Xia, H. Qiu, Q. Zhang, and C. Qiu, Tracking valley topology with synthetic weyl paths, *Physical Review Letters* **128**, 216403 (2022).
- [8] A. Rycerz, J. Tworzydło, and C. Beenakker, Valley filter and valley valve in graphene, *Nature Physics* **3**, 172 (2007).
- [9] J. Jung, F. Zhang, Z. Qiao, and A. H. MacDonald, Valley-hall kink and edge states in multilayer graphene, *Physical Review B* **84**, 075418 (2011).
- [10] F. Zhang, J. Jung, G. A. Fiete, Q. Niu, and A. H. MacDonald, Spontaneous quantum hall states in chirally stacked few-layer graphene systems, *Physical Review Letters* **106**, 156801 (2011).
- [11] D. Xiao, W. Yao, and Q. Niu, Valley-contrasting physics in graphene: magnetic moment and topological transport, *Physical Review Letters* **99**, 236809 (2007).
- [12] A. C. Neto, F. Guinea, N. M. Peres, K. S. Novoselov, and A. K. Geim, The electronic properties of graphene, *Reviews of modern physics* **81**, 109 (2009).
- [13] R. Gorbachev, J. Song, G. Yu, A. Kretinin, F. Withers, Y. Cao, A. Mishchenko, I. Grigorieva, K. S. Novoselov, L. Levitov, *et al.*, Detecting topological currents in graphene superlattices, *Science* **346**, 448 (2014).
- [14] X. Xu, W. Yao, D. Xiao, and T. F. Heinz, Spin and pseudospins in layered transition metal dichalcogenides, *Nature Physics* **10**, 343 (2014).
- [15] K. F. Mak, K. L. McGill, J. Park, and P. L. McEuen, The valley hall effect in mos2 transistors, *Science* **344**, 1489 (2014).
- [16] G. W. Semenoff, V. Semenoff, and F. Zhou, Domain walls in gapped graphene, *Physical Review Letters* **101**, 087204 (2008).
- [17] I. Martin, Y. M. Blanter, and A. Morpurgo, Topological confinement in bilayer graphene, *Physical Review Letters* **100**, 036804 (2008).
- [18] W. Yao, S. A. Yang, and Q. Niu, Edge states in graphene:

- From gapped flat-band to gapless chiral modes, *Physical Review Letters* **102**, 096801 (2009).
- [19] J. Li, A. F. Morpurgo, M. Büttiker, and I. Martin, Marginality of bulk-edge correspondence for single-valley hamiltonians, *Physical Review B* **82**, 245404 (2010).
- [20] J. Li, I. Martin, M. Büttiker, and A. F. Morpurgo, Topological origin of subgap conductance in insulating bilayer graphene, *Nature Physics* **7**, 38 (2011).
- [21] Z. Qiao, J. Jung, Q. Niu, and A. H. MacDonald, Electronic highways in bilayer graphene, *Nano Letters* **11**, 3453 (2011).
- [22] F. Zhang, A. H. MacDonald, and E. J. Mele, Valley chern numbers and boundary modes in gapped bilayer graphene, *Proceedings of the National Academy of Sciences* **110**, 10546 (2013).
- [23] A. Vaezi, Y. Liang, D. H. Ngai, L. Yang, and E.-A. Kim, Topological edge states at a tilt boundary in gated multilayer graphene, *Physical Review X* **3**, 021018 (2013).
- [24] L. Ju, Z. Shi, N. Nair, Y. Lv, C. Jin, J. Velasco, C. Ojeda-Aristizabal, H. A. Bechtel, M. C. Martin, A. Zettl, *et al.*, Topological valley transport at bilayer graphene domain walls, *Nature* **520**, 650 (2015).
- [25] J. Li, K. Wang, K. J. McFaul, Z. Zern, Y. Ren, K. Watanabe, T. Taniguchi, Z. Qiao, and J. Zhu, Gate-controlled topological conducting channels in bilayer graphene, *Nature Nanotechnology* **11**, 1060 (2016).
- [26] Z. Qiao, X. Li, W.-K. Tse, H. Jiang, Y. Yao, and Q. Niu, Topological phases in gated bilayer graphene: Effects of rashba spin-orbit coupling and exchange field, *Physical Review B* **87**, 125405 (2013).
- [27] M. Ezawa, Symmetry protected topological charge in symmetry broken phase: Spin-chern, spin-valley-chern and mirror-chern numbers, *Physics Letters A* **378**, 1180 (2014).
- [28] E. Fradkin, *Field theories of condensed matter physics* (Cambridge University Press, 2013).
- [29] P.-O. Löwdin, A note on the quantum-mechanical perturbation theory, *The Journal of Chemical Physics* **19**, 1396 (1951).
- [30] J. M. Luttinger and W. Kohn, Motion of electrons and holes in perturbed periodic fields, *Physical Review* **97**, 869 (1955).
- [31] G. L. Bir, G. E. Pikus, *et al.*, *Symmetry and strain-induced effects in semiconductors*, Vol. 484 (Wiley New York, 1974).
- [32] C. Xu, J. Wu, and C. Wu, Quantized interlevel character in quantum systems, *Physical Review A* **97**, 032124 (2018).
- [33] T. Holder, D. Kaplan, and B. Yan, Consequences of time-reversal-symmetry breaking in the light-matter interaction: Berry curvature, quantum metric, and diabatic motion, *Physical Review Research* **2**, 033100 (2020).
- [34] S. Kitamura, N. Nagaosa, and T. Morimoto, Nonreciprocal landau-zener tunneling, *Communications Physics* **3**, 1 (2020).
- [35] F. D. M. Haldane, Model for a quantum hall effect without landau levels: Condensed-matter realization of the " parity anomaly", *Physical Review Letters* **61**, 2015 (1988).
- [36] X. Zhang, W.-Y. Shan, and D. Xiao, Optical selection rule of excitons in gapped chiral fermion systems, *Physical Review Letters* **120**, 077401 (2018).
- [37] X. Zhang, *Topological Effects in Two-Dimensional Systems*, Ph.D. thesis, Carnegie Mellon University (2019).
- [38] M. S. Dresselhaus, G. Dresselhaus, and A. Jorio, *Group theory: application to the physics of condensed matter* (Springer Science & Business Media, 2007).
- [39] While γ can take on arbitrary integral values in graphene multilayers [36], we note that in monolayer MoS₂ and gapped topological surface states, $\alpha(|\mathbf{k}|) \propto |\mathbf{k}| = \sqrt{k_x^2 + k_y^2}$ (that is, $\gamma = 1$), and that in biased bilayer graphene, $\alpha(|\mathbf{k}|) \propto |\mathbf{k}|^2$ ($\gamma = 2$).
- [40] M. Fruchart and D. Carpentier, An introduction to topological insulators, *Comptes Rendus Physique* **14**, 779 (2013).
- [41] The factor of 2 is a peculiarity of 2-band models that arises from the Berry curvature sum rule $\sum_{i \in \text{all bands}} F_i = 0$, which guarantees us that the Berry curvature at each k -point of each band differs only by a sign. Therefore, the first two integrals in Eq. (2) simplify to a single integral with a factor of 2 (i.e., either $2 \int_{\mathcal{M}} F_n$ or $-2 \int_{\mathcal{M}} F_m$).
- [42] Recall that we used an overhead bar $\bar{\nu}^P$ in Eq. (3) to denote conventional definitions. ν^γ in Eq. (7) lacks an overhead bar to differentiate our novel contribution, which is quantized as a rational number.
- [43] The domain boundary could be between 1D strips separating a K -edge from a K' -edge. Or within one Brillouin zone, when inter-valley scattering is suppressed [5]..
- [44] C. W. Groth, M. Wimmer, A. R. Akhmerov, and X. Waintal, Kwant: a software package for quantum transport, *New Journal of Physics* **16**, 063065 (2014).
- [45] G.-B. Liu, W.-Y. Shan, Y. Yao, W. Yao, and D. Xiao, Three-band tight-binding model for monolayers of group-vib transition metal dichalcogenides, *Physical Review B* **88**, 085433 (2013).
- [46] J. Zhou, Q. Sun, and P. Jena, Valley-polarized quantum anomalous hall effect in ferrimagnetic honeycomb lattices, *Physical Review Letters* **119**, 046403 (2017).
- [47] H. Pan, Z. Li, C.-C. Liu, G. Zhu, Z. Qiao, and Y. Yao, Valley-polarized quantum anomalous hall effect in silicene, *Physical review letters* **112**, 106802 (2014).
- [48] M. Vila, J. H. Garcia, and S. Roche, Valley-polarized quantum anomalous hall phase in bilayer graphene with layer-dependent proximity effects, *Physical Review B* **104**, L161113 (2021).
- [49] T. Zhou, S. Cheng, M. Schleenvoigt, P. Schüffelgen, H. Jiang, Z. Yang, and I. Žutić, Quantum spin-valley hall kink states: From concept to materials design, *Physical Review Letters* **127**, 116402 (2021).
- [50] M. Koshino and E. McCann, Trigonal warping and berry's phase $n\pi$ in abc-stacked multilayer graphene, *Physical Review B* **80**, 165409 (2009).
- [51] W. Liu, Z. Lin, Z. Wang, and Y. Chen, Generalized haldane models on laser-coupling optical lattices, *Scientific Reports* **8**, 1 (2018).
- [52] D. Sticlet, F. Piéchon, J.-N. Fuchs, P. Kalugin, and P. Simon, Geometrical engineering of a two-band chern insulator in two dimensions with arbitrary topological index, *Physical Review B* **85**, 165456 (2012).
- [53] With the exception of [45], which remains an open problem.

Supplementary Material

A. Expanding the $d \arg$ term: deriving interband frequency

In this section, we explore Θ analytically using the mathematical relation $d \arg z = \text{Im} \frac{dz(\lambda)}{z(\lambda)}$ for $z(\lambda) \in \mathbb{C} \setminus \{0\}$. We now define the overhead dot $\dot{}$ and d to both denote derivation with respect to λ . To prove this relation, notice that $z = |z|e^{i \text{Arg}(z)}$ implies that $\log z = \log |z| + i \text{Arg}(z)$. Although Arg is defined only up to a constant multiple of 2π ($\equiv c$), this ambiguity disappears when we take the derivative: $\frac{d}{d\lambda} \arg(z) = \frac{d}{d\lambda} (\text{Im} \log \frac{z}{|z|} + c) = \text{Im} \frac{\dot{z}}{z}$. Note that the derivative of $\arg(z)$ is well-defined locally when $z \in \mathbb{C} \setminus \{0\}$. Consider a general N -level model with non-degenerate bands. Then, for $z(\lambda) = \langle m|\dot{n}\rangle$:

$$d \arg \langle m|\dot{n}\rangle = \text{Im} \frac{d \langle m|\dot{n}\rangle}{\langle m|\dot{n}\rangle}, \quad (\text{A1})$$

$$\text{and } \text{Im}(d \langle m|\dot{n}\rangle) = \text{Im}(\langle \dot{m}|n\rangle + \langle m|\ddot{n}\rangle).$$

Then, for levels $|m\rangle, |n\rangle$ and $|q\rangle$,

$$\begin{aligned} \langle \dot{m}|n\rangle &= \sum_q \langle \dot{m}|q\rangle \langle q|n\rangle \\ &= \langle \dot{m}|m\rangle \langle m|n\rangle + \langle \dot{m}|n\rangle \langle n|n\rangle + \sum_{q \neq m,n} \langle \dot{m}|q\rangle \langle q|n\rangle \\ &= -\langle m|\dot{m}\rangle \langle m|n\rangle - \langle m|\dot{n}\rangle \langle n|n\rangle - \sum_{q \neq m,n} \langle m|\dot{q}\rangle \langle q|n\rangle \\ &= \langle m|\dot{n}\rangle \left[i\mathcal{A}_m + i\mathcal{A}_n - \sum_{q \neq m,n} \frac{\langle m|\dot{q}\rangle \langle q|n\rangle}{\langle m|\dot{n}\rangle} \right], \end{aligned}$$

where we used the definition for the Berry connection $\langle a|\dot{a}\rangle = -i\mathcal{A}_a$ and the relation $d \langle a|b\rangle = d(0)$ implies that $\langle \dot{a}|b\rangle = -\langle a|\dot{b}\rangle$ for orthonormal states $\{|a\rangle, |b\rangle\}$.

To treat the last term in (A1), recall that for any two functions f, g of λ , the second derivative is $d^2(fg) = (d^2f)g + 2(df)(dg) + f(d^2g)$. Applying this to Schrödinger's equation $H|n\rangle = E_n|n\rangle$ gives:

$$\ddot{E}_n|n\rangle + 2\dot{E}_n|\dot{n}\rangle + E_n|\ddot{n}\rangle = \ddot{H}|n\rangle + 2\dot{H}|\dot{n}\rangle + H|\ddot{n}\rangle.$$

Applying ket $\langle m|$, using $\langle m|n\rangle = 0$ and the notation $E_{nm} = E_n - E_m$:

$$\langle m|\ddot{n}\rangle = \frac{\langle m|\dot{n}\rangle}{E_{nm}} \left(-2\dot{E}_n + \frac{\langle m|\ddot{H}|n\rangle}{\langle m|\dot{n}\rangle} + 2\frac{\langle m|\dot{H}|\dot{n}\rangle}{\langle m|\dot{n}\rangle} \right).$$

For a general N -level Hamiltonian, the numerator of the last term above becomes:

$$\begin{aligned} \langle m|\dot{H}|\dot{n}\rangle &= \sum_q \langle m|\dot{H}|q\rangle \langle q|\dot{n}\rangle \\ &= \langle m|\dot{H}|m\rangle \langle m|\dot{n}\rangle + \langle m|\dot{H}|n\rangle \langle n|\dot{n}\rangle + \sum_{q \neq m,n} \langle m|\dot{H}|q\rangle \langle q|\dot{n}\rangle. \end{aligned}$$

Using the Hellman-Feynman-type relation $\langle m|\dot{H}|n\rangle =$

$E_{nm} \langle m|\dot{n}\rangle$, the above

$$= \langle m|\dot{n}\rangle \left(\langle m|\dot{H}|m\rangle + E_{nm} \langle n|\dot{n}\rangle + \sum_{q \neq m,n} E_{qm} \frac{\langle m|\dot{q}\rangle \langle q|\dot{n}\rangle}{\langle m|\dot{n}\rangle} \right).$$

For $\beta = \{\langle m|\dot{H}|m\rangle\}$ with $\dot{E}_n \in \mathbb{R}$, we have $\text{Im}(\beta) = 0$. Finally, we get:

$$\begin{aligned} &\text{Im} \frac{d \langle m|\dot{n}\rangle}{\langle m|\dot{n}\rangle} \\ &= \mathcal{A}_m - \mathcal{A}_n + \text{Im} \frac{\langle m|\ddot{H}|n\rangle}{\langle m|\dot{H}|n\rangle} \\ &\quad + \sum_{q \neq m,n} \text{Im} \frac{\langle m|\dot{q}\rangle \langle q|\dot{n}\rangle}{\langle m|\dot{n}\rangle} \left(2\frac{E_{qm}}{E_{nm}} - 1 \right) \\ &= \mathcal{A}_m - \mathcal{A}_n + \text{Im} \frac{\langle m|\ddot{H}|n\rangle}{\langle m|\dot{H}|n\rangle} \\ &\quad + \sum_{q \neq m,n} \text{Im} \frac{\langle m|\dot{H}|q\rangle \langle q|\dot{H}|n\rangle}{\langle m|\dot{H}|n\rangle} \left(\frac{2}{E_{nq}} - \frac{E_{nm}}{E_{qm}E_{nq}} \right). \end{aligned}$$

When plugged into Eq. (1), we get Eq. (2) given in the main text.

B. Berry curvature of gapped Dirac model

Using Eq. (4), the Berry curvature of the gapped Dirac fermion model is calculated as [5]:

$$\frac{\gamma\omega\Delta\alpha^2|k|^{2(\gamma-1)}}{2(\Delta^2 + \alpha^2|k|^{2\gamma})^{3/2}}. \quad (\text{B1})$$

Figure 4 shows the Berry curvature distribution to supplement the argument around Fig. 1 (d). Notice that the Berry curvature sums to $\approx 1.5 \times 2\pi \text{ \AA}^{-2}$.

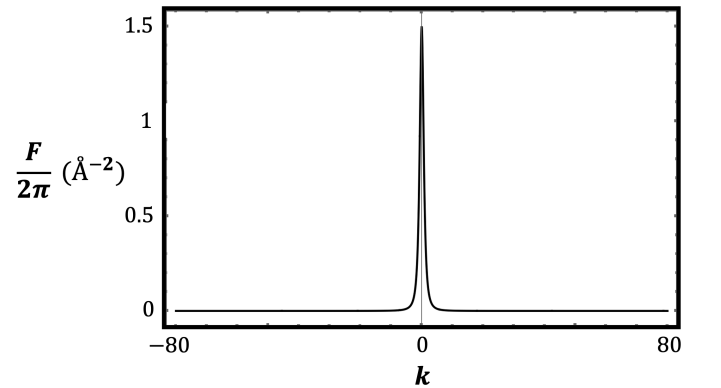


FIG. 4: Berry curvature of the gapped Dirac fermion model along the line $k_y = 0$. This is the same case as in Fig. 1 (d), where varying r from 0 to 80 encompasses $-80 \leq k_x \leq 80$.

C. Models used; and definitions of first, valley, spin and spin-valley Chern numbers

We tested the following $k \cdot p$ models: 2-band gapped Dirac fermion model [36]; 4-band gapped bilayer graphene with layer-stacking wall [22]; 4-band spinful Dirac Hamiltonian on monolayer honeycomb lattice [27]; 4-band ferrimagnetic honeycomb lattice model for the valley-polarized quantum anomalous Hall effect [46] (see also [47–49]); 6-band ABC-Stacked trilayer graphene [50]; 8-band gated bilayer graphene with Rashba spin-orbit coupling and exchange field ([26], F). We tested the following lattice models: Haldane model for the quantum anomalous Hall effect [35]; the 3-band model in [51]; and models allowing $|C| > 1$, even if they have more than 2 high-symmetry points P beyond K and K' (such as in [52]).

We note that electron-hole symmetry is not necessary for our conclusions to hold. We verified this using the 3-band model [51], which inherently lacks electron-hole symmetry.

To define existing topological indices using a specific example, consider a spinful system with only two P (K, K') for each spin label (\uparrow, \downarrow). This could be the Dirac Hamiltonian on a monolayer honeycomb lattice [27]. Then, per [27], the first, valley, spin, and spin-valley Chern numbers are respectively:

$$\begin{aligned} C &= \nu^{K,\uparrow} + \nu^{K',\uparrow} + \nu^{K,\downarrow} + \nu^{K',\downarrow} \\ V &= (\nu^{K,\uparrow} + \nu^{K,\downarrow}) - (\nu^{K',\uparrow} + \nu^{K',\downarrow}) \\ 2C_s &= (\nu^{K,\uparrow} + \nu^{K',\uparrow}) - (\nu^{K,\downarrow} + \nu^{K',\downarrow}) \\ 2C_{sv} &= (\nu^{K,\uparrow} + \nu^{K',\downarrow}) - (\nu^{K',\uparrow} + \nu^{K,\downarrow}). \end{aligned} \quad (C1)$$

Under certain symmetries, the \mathbb{Z}_2 index for topological insulators = $C_s \pmod{2}$ [27]. For all models tested [53], we recovered the expected topological quantities (C1). For instance, we got the $N\pi$ Berry phases for the N -layer graphene models, and the V in [22]. Results not included in this paper may be requested from the authors upon reasonable request.

D. Showing $\Theta^{mn} = -\Theta^{nm}$

First we consider $\Delta\Phi$ in (1): $\Delta\Phi^{mn} = \Phi_m - \Phi_n = -(\Phi_n - \Phi_m) = -\Delta\Phi^{nm}$. Next, we consider the term $\langle m|\dot{n}\rangle$ (using the λ formulation for simplicity). Notice that: $d(0) = d(\langle m|n\rangle) = \langle \dot{m}|n\rangle + \langle m|\dot{n}\rangle = 0$. It follows that $\langle \dot{m}|n\rangle = -\langle m|\dot{n}\rangle$. Putting all this together, we get $\Theta^{mn} = -\Theta^{nm}$.

E. Choosing k -space loops

In the main text, we considered Ξ_n^P per high-symmetry point P . This means that loops used to calculate Ξ must enclose only one special point P . Based on our numeri-

cal results, these P are high-symmetry points associated with crystal symmetry (such as $K, K', M, \Gamma, X, \dots$). They may not necessarily be points where the band gap may close. We observe that the interband matrix element $\langle m|\nabla_{\mathbf{k}}n\rangle \cdot \hat{e}_\tau$ (1) diverges at these P . However, due to the matrix element's gauge-dependence, we doubt that this observation can be used to identify P . This is also due to the fact that, in a non-azimuthal basis, we do not have a unique k -space vector field prior to choosing a loop. Otherwise, its critical points may have been used to identify P . We get the results in this work only for loops enclosing high-symmetry points. Why these points P are important remains an open question.

Another numerical observation is that the winding loop of the interband matrix element is coincidentally discontinuous if the k -space loop does not include only Berry curvature F of only one sign. Our numerical implementation demonstrated this discontinuity also when the band is gapless anywhere in parameter space (not necessarily inside or along the loop). This is very likely a numerical artefact. Our calculations also indicate that loops not enclosing aforementioned high-symmetry points P may only yield $\Theta = \pm 1$. In 2-band models, we see that $\Theta \propto \text{sign}(F)$ of the region within the loop.

F. Gated bilayer graphene with Rashba spin-orbit coupling and exchange field

Ref. [26] gives the following momentum space 8-band effective Hamiltonian for the valley points K and K' (centered at the origin $(0, 0)$ and respectively labeled by $\eta = \pm 1$):

$$\begin{aligned} \mathbf{H}(\mathbf{k}) &= v(\eta\sigma_z k_x + \sigma_y k_y)\mathbf{1}_s\mathbf{1}_\tau + \frac{t_\perp}{2}(\sigma_x\tau_x - \sigma_y\tau_y)\mathbf{1}_s \\ &+ \frac{\lambda_R}{2}(\eta\sigma_x s_y - \sigma_y s_x)\mathbf{1}_\tau + M s_z\mathbf{1}_\sigma\mathbf{1}_\tau + U\tau_z\mathbf{1}_s\mathbf{1}_\tau, \end{aligned} \quad (F1)$$

where s, σ and τ are Pauli matrices representing the spin, AB sublattice, and top-bottom layer degrees of freedom respectively. $\mathbf{1}_i$ are 2×2 identity matrices. The Fermi velocity is given by $v = 3at/2$ with a the lattice constant, and t the hopping amplitude. t_\perp is the interlayer tunneling amplitude, λ_R the Rashba spin-orbit coupling, U the interlayer potential, and M the exchange field. We used $a = 1, t = 2.6, t_\perp = 0.143t, M = 0, U = 0.3t$ and $t_R = 0.058t$.

We ignored the exchange field M in our calculations for simplicity in presentation. However, using $M \neq 0$, we were able to reproduce the phase diagrams in Ref. [26] which classify quantum anomalous Hall, quantum valley Hall, and metallic phases (c.f. Figure 15 of the reference).

For our numerical calculations, we used *MATLAB* and *Python*. We used k -loops discretized to 250 segments, and a 100×100 k -grid.